Scattering of nitrogen molecules by silver atoms

Scattering of nitrogen molecules by silver atoms

Jérôme Loreau,[1,a)] Peng Zhang,[1,2] and Alexander Dalgarno[1]
[1]*Institute for Theoretical Atomic, Molecular and Optical Physics (ITAMP), Harvard-Smithsonian Center for Astrophysics, Cambridge, Massachusetts 02138, USA*
[2]*Department of Chemistry, Duke University, Durham, North Carolina 27708, USA*

(Received 24 February 2012; accepted 29 March 2012; published online 25 April 2012)

We present a quantal study of the rotationally elastic and inelastic scattering of Ag and N_2, with the nitrogen molecule treated as a rigid rotor. The two-dimensional potential energy surface of the AgN_2 complex is obtained *ab initio* by means of the spin unrestricted coupled-cluster method with single, double, and perturbative triple excitations. The global minimum is found to be located at an internuclear distance of 8.13 a_0 and an angle of 127.2°. The long-range part of the potential is constructed from the dynamic electric dipole polarizabilities of Ag and N_2. Elastic, excitation, and relaxation cross sections and rates are calculated for energies between 0.1 and 5000 cm^{-1}. The momentum transfer cross sections and rates are also computed. Finally, we compare the cross sections for Ag–N_2 and Na–N_2 to explore the possibility of using silver instead of sodium in experimental tests.
 [http://dx.doi.org/10.1063/1.3703518]

I. INTRODUCTION

Sodium laser guide stars are currently in operation or under development at major ground-based telescopes in order to improve the use of adaptive optics. One of the major difficulties in their implementation is the modeling of the photon return from the sodium layer present in the mesosphere. In particular, collisions of Na with N_2, O, and O_2 and spin exchange collisions with O_2 change the velocity of the sodium atoms, hence, these processes must be included in theoretical models in order to optimize the return flux.[1] In addition, it is also important to consider the effects of these collisions in the context of the use of mesospheric sodium in remote-detection magnetometry.[2] We have recently performed a theoretical investigation of Na–N_2 collisions using the close-coupling method for temperatures between 100 and 300 K,[3] but the cross sections for collisions of Na with O and O_2 are still unknown. Furthermore, the experimental determination of these cross sections is very challenging due to the high reactivity of sodium. Due to its low chemical reactivity, and because their electronic structure are similar (in the ground state, a single *s* electron outside a filled shell), silver has been proposed as a possible substitute for sodium in experiments.[4]

Silver atoms ablated into a dense buffer gas such as He or N_2 at temperatures ranging from a few K to room temperature have been explored experimentally and proposed as a potential system for a high-sensitivity cryogenic atomic magnetometer.[5] Ag–N_2 collisions could also have applications in the context of spin-exchange optical pumping (SEOP). It has been recently demonstrated theoretically that the rate of spin polarization of ^{3}He can be improved by the use of Ag instead of alkali-metal atoms.[6] A typical SEOP experiment consists of a cell containing an alkali-metal and a noble gas. The alkali-metal is spin polarized by optical pumping, and the spin polarization is transferred to the noble gas during collisions.[7] The cell also contains N_2, which is used to quench the excited atoms, and the interaction of nitrogen with the alkali-metal can have important effects on the SEOP mechanism.[8]

The purpose of this work is to describe Ag–N_2 collisions using a fully quantal method. In Sec. II, we present the two-dimensional potential energy surface of the ground state of the AgN_2 van der Waals complex, calculated using *ab initio* methods with the N_2 molecule frozen in its equilibrium geometry. In Sec. III, we calculate the elastic and inelastic (excitation and de-excitation) rotational cross sections, as well as the differential and momentum transfer cross sections, for energies in the range 0.1–5000 cm^{-1}. We also calculate the corresponding rate constants for temperatures between 1 K and 1000 K, and we compare these results to the calculations recently reported on Na–N_2 scattering[3] to investigate the possibility of using Ag as a substitute for Na in experimental tests.

II. *AB INITIO* CALCULATIONS

A. Interaction potential

To parametrize the potential energy surface of the AgN_2 complex, we used the three standard Jacobi coordinates (R, r, θ). R is the distance between the silver atom and the center of mass of the N_2 molecule, r denotes the length of the N–N bond, and θ is the angle between R and r. As the first excited vibrational state of N_2 lies about 2330 cm^{-1} above the ground state,[9] vibrational excitation is not expected to contribute significantly. The internuclear distance of N_2 is therefore fixed to the equilibrium geometry, $r = 2.4132$ a.u. The ground state configuration of the silver atom is $4d^{10}5s^1\,{}^2S$, while the ground state of the nitrogen molecule is a $^1\Sigma_g^+$ state. Therefore, the ground state of the AgN_2 van der Waals complex corresponds to the $^2A'$ representation of the symmetry group C_s. For the particular geometries $\theta = 0°$ (linear) and

a)Electronic mail: jloreau@cfa.harvard.edu.

$\theta = 90^\circ$ (T-shaped), the ground state will be, respectively, a $^2\Sigma^+$ or a $^2A_1$ state.

The two-dimensional potential energy surface (PES) of the ground state was calculated using the spin unrestricted coupled-cluster method with single, double, and perturbative triple excitations (UCCSD(T))[10,11] implemented in the MOLPRO 2009.1 package.[12] The reference wave function employed in the CC calculations was generated from the spin restricted Hartree-Fock method. For the Ag atom, we used the cc-pwCVQZ-PP basis set.[13] This basis set consists of a small-core relativistic pseudopotential, which replaces the $1s - 3d$ core and includes scalar and spin-orbit effects,[14] and of a quadruple zeta basis set for the valence electrons, including valence plus core-valence correlation. This basis set was augmented by diffuse functions[13] (one for each angular momentum symmetry) to accurately describe the weakly bound complex AgN_2. For the N atoms, the aug-cc-pwCVQZ basis set[15] was used. In our calculations, we treated the $1s^2$ electrons of both N atoms as core electrons. In total, 29 electrons (the $4s^2 4p^6 4d^{10} 5s^1$ electrons of the Ag atom and the $2s^2 2p^3$ electrons of the N atoms) were correlated explicitly in the UCCSD(T) calculations.

We constructed the two-dimensional PES $V(R, \theta)$ using an uniform grid of 583 geometries. The grid for the intermolecular distance is $3.4 \leq R \leq 19$ a.u. with a step-length of 0.3 a.u. while for the θ we used a grid $90^\circ \leq \theta \leq 180^\circ$ with a step size of 10°, with an additional series of points at $\theta = 95^\circ$. The potential for $0^\circ \leq \theta < 90^\circ$ is obtained by symmetry with respect to $\theta = \pi/2$. For each geometry, the energy was corrected to account for the basis set superposition error (BSSE) using the counterpoise method.[16]

The *ab initio* potential energy surface $V(R, \theta)$ is shown in Fig. 1. It is strongly repulsive at distances smaller than 6 a.u., and weakly attractive for large R. The potential has a global minimum at $\theta = 127.2^\circ$ (and at $\theta = 52.8^\circ$) and the equilibrium distance is $R = 8.13$ a.u., with a dissociation energy $D_e = 81.8$ cm^{-1}. As can be seen from Fig. 1, the potential has a saddle point at $\theta = 90^\circ$. The dissociation energy of this configuration is 73.1 cm^{-1}, 8.7 cm^{-1} above the global minimum, and corresponds to the intermolecular distance $R = 8.07$ a.u. In the linear geometry ($\theta = 0^\circ$ or 180°), the minimum of the potential is shifted toward larger intermolecular distances ($R = 8.83$ a.u.) and the dissociation energy is 67.0 cm^{-1}. The distances R for which the interaction energy is maximal are given in Table I for a series of angles. In particular, we observe that the equilibrium distance increases as the complex approaches the linear configuration. The effect of the BSSE on the dissociation energy at the global minimum is about 12 cm^{-1}.

B. Long-range interactions

The asymptotic long-range attractive potential V_{as} is dominated by the dispersion forces and can be constructed in an analytical form. We retain here the leading term,

$$V_{as} = -\frac{C_6}{R^6}\,. \tag{1}$$

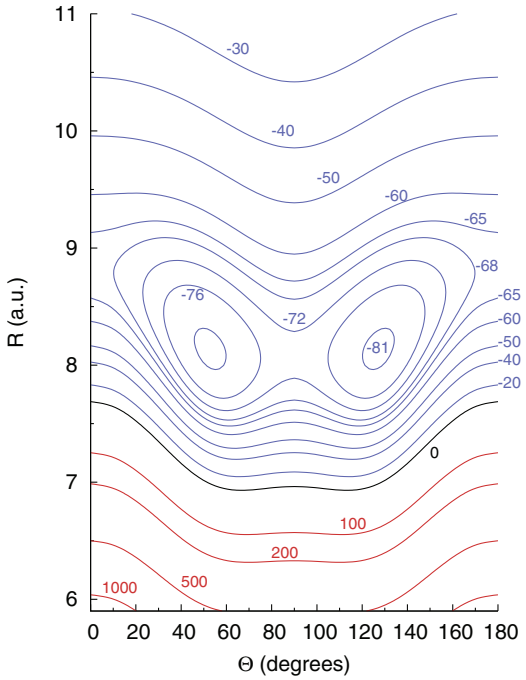

FIG. 1. Contour plot of the potential energy surface $V(R, \theta)$ for the AgN_2 complex. The energies are in units of cm^{-1}.

In the case of the interaction between an S-state atom and a linear molecule, the C_6 coefficient is given by the sum of an isotropic and an anisotropic component,[17]

$$C_6 = C_{6,0} P_0(\cos\theta) + C_{6,2} P_2(\cos\theta), \tag{2}$$

where P_0 and P_2 are the Legendre polynomials of order 0 and 2, respectively. The isotropic and anisotropic dispersion coefficients may be derived using the dynamic electric dipole polarizabilities as

$$C_{6,0} = \frac{3}{\pi}\int_0^\infty \alpha^{Ag}(i\omega)\overline{\alpha}^{N_2}(i\omega)d\omega, \tag{3}$$

$$C_{6,2} = \frac{1}{\pi}\int_0^\infty \alpha^{Ag}(i\omega)\left[\alpha_\parallel^{N_2}(i\omega) - \alpha_\perp^{N_2}(i\omega)\right]d\omega\,, \tag{4}$$

TABLE I. Equilibrium distances of the Ag–N_2 potential $V(R, \theta)$ for various values of θ and with $r = 2.4132$ a.u., and corresponding dissociation energies D_e. $\theta = 127.2^\circ$ is the global minimum of the potential.

θ (deg)	R (a.u.)	D_e (cm^{-1})
90	8.07	73.1
100	8.06	74.5
110	8.06	77.8
120	8.07	81.0
127.2	8.13	81.8
130	8.16	81.7
140	8.31	79.2
150	8.50	75.0
160	8.67	70.8
170	8.79	68.0
180	8.83	67.0

TABLE II. Parameters of the switching function (5).

a	*b*	*c*	*d*
−0.0216922	0.717031	0.124343	19.6663

where $\alpha_\parallel(i\omega)$ and $\alpha_\perp(i\omega)$ are, respectively, the longitudinal and transverse dynamical electric dipole polarizabilities, evaluated as functions of imaginary frequencies $i\omega$, while $\overline{\alpha}$ is the average dipole polarizability, $\overline{\alpha} = \frac{1}{3}(\alpha_\parallel + 2\alpha_\perp)$. The expressions (3) and (4) can be calculated efficiently using Gaussian quadrature.[18] As in Ref. 3, the dynamic polarizabilities of the N_2 molecule were evaluated using the time-independent linear response coupled-cluster theory[19] at the third-order in the fluctuation potential, as implemented in MOLPRO, and a triply augmented correlation consistent polarized core-valence sextuple zeta (t-aug-cc-pCV6Z) basis set.[20]

For the Ag atom, we adopted the accurate values reported in Ref. 21, which include core contributions. The integration was realized using a 50-point Gaussian quadrature, and we obtained $C_{6,0}$=147.56 a.u. and $C_{6,2}$=17.47 a.u. The accuracy of these dispersion coefficients can be further verified through direct comparison with the *ab initio* UCCSD(T) calculations. Substituting the values of the C_6 coefficients into Eq. (1), we find that the energy difference between the UCCSD(T) calculations and the asymptotic potential (1) at the last point of our computed grid (R = 19 a.u.) is smaller than 0.2 cm^{-1}, the largest difference occurring for the linear geometry ($\theta = 180°$). In order to smoothly connect the *ab initio* points and the asymptotic potential, we used a switching function expressed as the product of an R-dependent and a θ-dependent function. It is given by

$$f(R,\theta) = -(1+\tanh(aR+b))\cos(c(\theta+d)). \quad (5)$$

The four parameters a, b, c, d were optimized with respect to the *ab initio* points at large R using a nonlinear least-squares Marquardt-Levenberg algorithm and are given in Table II. The root mean square deviation was 3×10^{-3} cm^{-1}. A cubic spline method was employed to generate the potential for R < 19 a.u.

In scattering calculations, it is often useful to expand the intermolecular potential $V(R,\theta)$ in terms of Legendre polynomials of order λ in order to simplify the evaluation of its matrix elements,

$$V(R,\theta) = \sum_\lambda V_\lambda(R) P_\lambda(\cos\theta)\,, \quad (6)$$

where the $V_\lambda(R)$ are known as "radial strength functions". The first four radial functions $V_\lambda(R)$ are shown in Fig. 2. Only even values of λ appear in (6) due to the symmetry of the intermolecular potential.

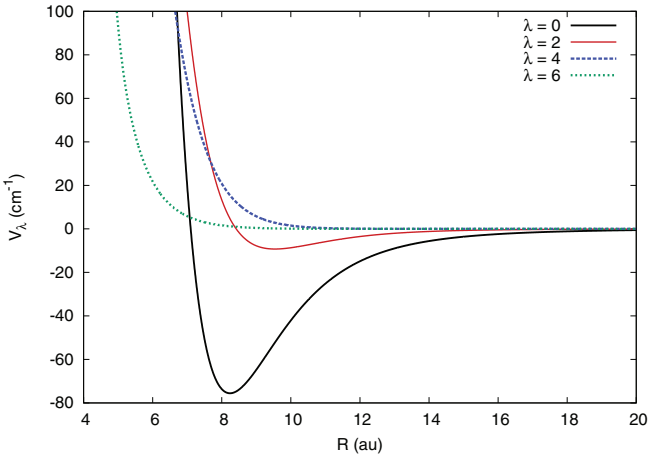

FIG. 2. The first four radial functions $V_\lambda(R)$ in the expansion (6) of the intermolecular potential $V(R,\theta)$.

III. SCATTERING CALCULATIONS

A. Computational method

We calculated the cross sections for Ag–N_2 collisions using the quantum close-coupling method developed by Arthurs and Dalgarno,[22] which has been described extensively in the literature.[23] N_2 was held fixed at its equilibrium bond-length and treated in the rigid-rotor approximation. We represented the energy of the rotational levels of the nitrogen $^1\Sigma_g^+$ ground state using the rotational constants of N_2 given in Refs. 9 and 24,

$$B_e = 1.99824\ \text{cm}^{-1}\,, \qquad D_e = 5.76\cdot 10^{-6}\ \text{cm}^{-1}\,,$$
$$\alpha_e = 0.017318\ \text{cm}^{-1}\,.$$

In the close-coupling method, the total wave function of the Ag–N_2 complex is expanded as a sum of products of radial and rotational functions. When inserted in the Schrödinger equation, this leads to a set of second-order coupled differential equations for the radial functions that must be solved with appropriate boundary conditions. In these equations, the coupling between the different channels is represented by matrix elements of the intermolecular potential. It is convenient to introduce the total angular momentum $\mathbf{J} = \mathbf{j} + \mathbf{l}$, where $\mathbf{j}$ is the angular momentum of N_2 and $\mathbf{l}$ is the orbital momentum. The total angular momentum is conserved during the collision, so that the coupled equations are block-diagonal in J. The S matrix elements $S^J_{j'l'jl}$ can then be obtained from the asymptotic behavior of the radial functions, and the cross section for the transition from an initial rotational state j to a final rotational state j' is given in terms of the S matrix elements as

$$\sigma_{j\to j'} = \frac{\pi}{(2j+1)k_j^2}\sum_{J=0}^{\infty}\sum_{l=|J-j|}^{|J+j|}\sum_{l'=|J-j'|}^{|J+j'|} \times (2J+1)|\delta_{jj'}\delta_{ll'} - S^J_{j'l'jl}|^2, \quad (7)$$

where $k_j^2 = 2\mu E_c = 2\mu(E-\epsilon_j)$ is the wavenumber in the entrance channel with energy ϵ_j, E_c is the kinetic energy, and E is the total (kinetic plus rotor) energy.

In addition to the integral cross section, the properties of the atom-molecule collision are also determined by the momentum transfer cross section $\sigma^{\text{tr}}_{j\to j'}$ (or transport cross section). The momentum transfer cross section from an initial level j to a final level j' is obtained from the differential cross

sections $d\sigma/d\Omega$ as[25]

$$\sigma^{\rm tr}_{j\to j'}(E_c) = 2\pi \int \frac{d\sigma_{j\to j'}(E_c,\gamma)}{d\Omega} \sin\gamma\, \Phi(E_c,\gamma) d\gamma\ , \quad (8)$$

where γ is the scattering angle. It differs from the integral cross section given by Eq. (7) by the function

$$\Phi(E_c,\gamma) = 1 - \sqrt{E'_c/E_c}\cos\gamma\ , \quad (9)$$

where E'_c is the final kinetic energy, related to the initial kinetic energy by

$$E'_c = E_c + \epsilon_j - \epsilon_{j'}. \quad (10)$$

The thermal rate coefficient for a transition $j \to j'$ at a given temperature T is given by the integral of the cross section over a Maxwell-Boltzmann distribution of initial energies

$$k_{j\to j'}(T) = \left(\frac{2}{k_B T}\right)^{3/2} \frac{1}{\sqrt{\pi\mu}} \int_0^\infty E_c e^{-E_c/k_B T} \sigma_{j\to j'}(E_c)\, dE_c, \quad (11)$$

where k_B is the Boltzmann constant. The rate coefficient for momentum transfer, $k^{\rm tr}(T)$, is given by the same expression, replacing $\sigma(E_c)$ by $\sigma^{\rm tr}(E_c)$.

We carried out the scattering calculations for collision energies between 0.1 and 5000 cm^{-1} using the nonreactive scattering code MOLSCAT of Hutson and Green.[26] The radial equations were solved using a hybrid modified log-derivative Airy propagator.[27] The log-derivative matrix is propagated on a grid of intermolecular distances between $R_{\rm min}$ and $R_{\rm max}$, where the numerical calculations are matched with the asymptotic solutions and the S matrix elements are extracted. We used a grid starting at $R_{\rm min} = 3$ a.u., while the $R_{\rm max}$ was in the range 70–150 a.u., depending on the energy of collision. For a particular energy, the propagation is carried out until convergence of the sum over the total angular quantum number J in Eq. (7) is achieved.

B. Cross sections

In this section, we present the integral and momentum transfer cross sections for elastic and rotationally inelastic transitions. The elastic and inelastic integral cross sections starting from the initial rotational levels $j = 1$, $j = 5$, and $j = 10$ are shown in Figs. 3–5 for energies between 0.1 and 5000 cm^{-1}. We observe resonance structures in the elastic cross section for the initial rotational level $j = 1$, as well as in the inelastic cross sections from $j = 1$ to $j' = 3$ and $j' = 5$, for energies below the depth of the van der Waals potential ($\sim$80 cm^{-1}). These resonances at low kinetic energy are a consequence of the attractive potential well, which allows Ag to be temporarily trapped and hence quasi-bound states to be formed. These states may arise from the tunneling from the centrifugal barrier and from excitation of N_2 to an asymptotically closed channel where N_2 becomes temporarily trapped in one of the bound states of the potential well.[28–30] Compared to the depth of the potential well, the energy spacing of the N_2 rotational structure is small, so that both types of quasi-bound states occur in the same energy range. Although the resonances are still present for the initial rotational levels

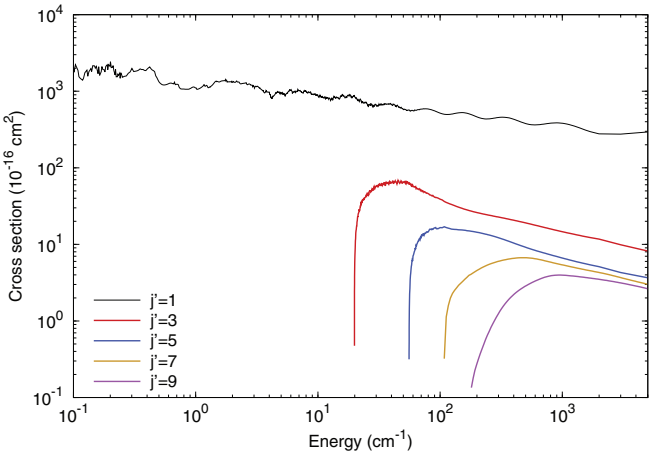

FIG. 3. Elastic and inelastic cross sections $\sigma_{j\to j'}$ for the initial rotational level $j = 1$ and the final rotational levels $j' = 1 - 9$.

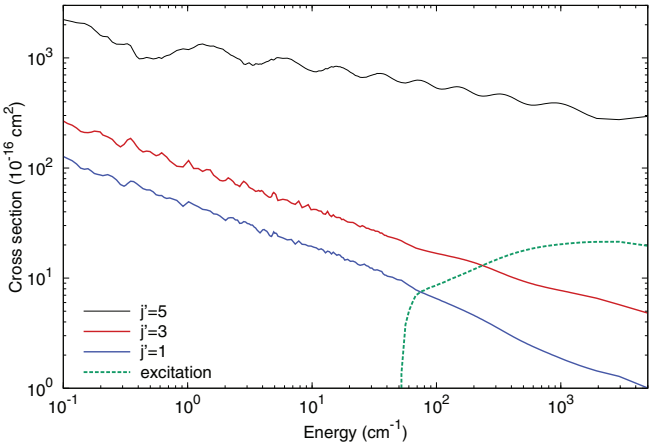

FIG. 4. Elastic and inelastic cross sections $\sigma_{j\to j'}$ for the initial rotational level $j = 5$. The excitation cross section is the sum of the cross sections over all rotational levels $j' > j$.

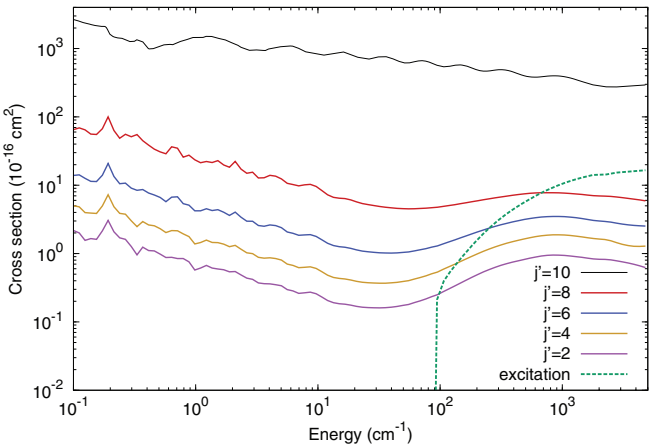

FIG. 5. Elastic and inelastic cross sections $\sigma_{j\to j'}$ for the initial rotational level $j = 10$. The excitation cross section is the sum of the cross sections over all rotational levels $j' > j$.

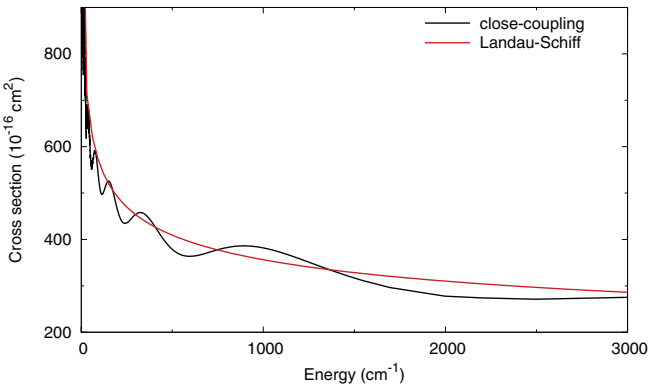

FIG. 6. Elastic cross sections for $j = 1$ and comparison with the Landau-Schiff formula, Eq. (12).

$j = 5$ and $j = 10$ (see Figs. 4 and 5), they are gradually suppressed with increase in the initial rotational level, as the van der Waals potential well supports only a limited number of excited quasi-bound levels. Levels corresponding to higher j therefore become virtual states producing no resonances.

In addition to the resonance structure for energies below 80 cm^{-1}, the elastic cross sections present undulations as a function of the kinetic energy. These undulations are present for all initial rotational levels, and the position of the maxima is almost independent of j. This peak structure is characteristic of glory undulations,[31] and the independence of the peak positions with respect to the initial rotational state indicates that the rotational time of N_2 is short compared to the characteristic translational time. The elastic cross sections are very similar for all initial rotational levels, although for energies below 80 cm^{-1}, there can be significant differences due to the resonance structure. They become comparable at higher energies, but for a given energy the cross section increases slightly with j. At 100 cm^{-1}, the $j = 5$ and $j = 15$ cross sections are larger than the $j = 1$ cross section by about 3% and 6%, respectively, while the difference drops to 1% and 5% at 1000 cm^{-1}.

The elastic cross section can be estimated from the semi-classical Landau-Schiff formula for scattering by a R^{-n} potential,[32]

$$\sigma = 2\pi^{\frac{n}{n-1}} \sin\left[\frac{\pi}{2}\frac{n-3}{n-1}\right]\Gamma\left[\frac{n-3}{n-1}\right]\left(\frac{\Gamma[\frac{n-1}{2}]}{\Gamma[\frac{n}{2}]}\right)^{\frac{2}{n-1}}\left(\frac{C_n}{v}\right)^{\frac{2}{n-1}}. \quad (12)$$

The Landau-Schiff elastic cross section, computed from the C_6 coefficient presented in Sec. II B, is shown in Fig. 6. We observe a very good agreement with the close-coupling calculations for the rotational state $j = 1$ illustrated in the figure. As the elastic cross sections are similar for all initial rotational levels, the agreement is valid for all values of j.

Over the range of energies considered in this work, the collision is mostly elastic. As can be seen from Figs. 3–5, the inelastic cross sections are roughly an order of magnitude smaller than the elastic. At low energy, the inelastic process is dominated by the relaxation to the rotational level $j' = j - 2$. At higher energy, when several excited rotational levels become energetically available, the inelastic transitions are dominated by excitation into the rotational levels $j' > j$. The rotational relaxation occurs preferentially through

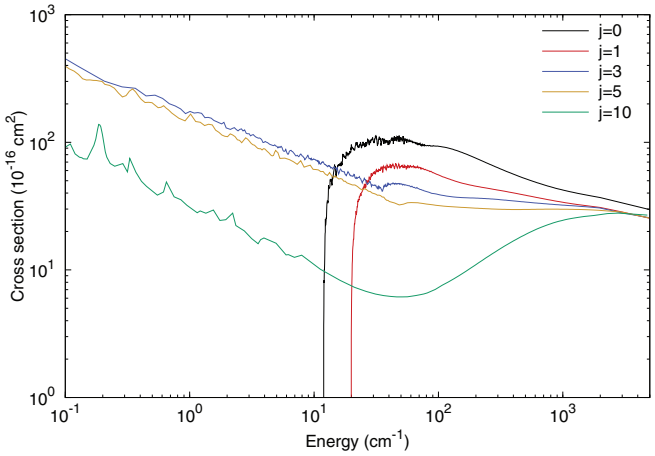

FIG. 7. Total rotationally inelastic cross section $\sum_{j' \neq j} \sigma_{j \to j'}$ for several initial rotational levels j.

the highest rotational level for all energies. In Fig. 7, we compare the total inelastic (relaxation plus excitation) cross sections for various initial rotational levels. We observe that for a given energy, the inelastic cross sections decrease with increasing initial rotational level. However, at high energies (above 1000 cm^{-1}), the cross section includes contributions from many rotational levels and the inelastic cross section becomes independent of the initial rotational state.

The elastic and inelastic momentum transfer cross sections $\sigma^{\rm tr}_{j \to j'}$, given by Eq. (8) are presented in Fig. 8 for the initial levels $j = 1$, $j = 5$, and $j = 10$. For energies below the depth of the potential, the elastic cross sections for the various initial rotational levels can be quite different. However, at higher energies they all converge towards the same value. The elastic momentum transfer cross sections are smaller than the elastic integral cross sections at all energies, due to the function $\Phi(E_c, \gamma) = 1 - \sqrt{E'_c/E_c}\cos\gamma$ (see Eq. (9)), which suppresses the contributions from the small angles (forward scattering) in the differential cross section. The difference between the two types of elastic cross sections increases with the energy. This is due to the fact that at low energy, the

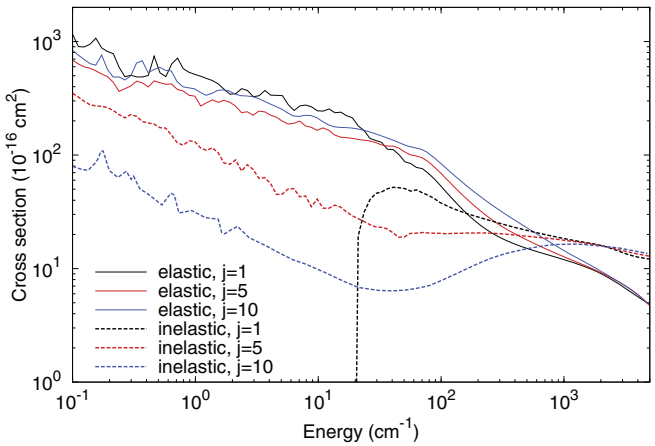

FIG. 8. Momentum transfer cross sections for the initial levels $j = 1$, $j = 5$, and $j = 10$. Full lines, elastic cross sections; dashed lines, inelastic cross sections.

differential cross section is large for all scattering angles. However, as the energy increases, the contributions from large γ decrease rapidly and the collisions are dominated by forward scattering. Therefore, the momentum transfer cross sections $\sigma^{\rm tr}_{j\to j'}$ decrease more quickly than the integral cross sections $\sigma_{j\to j'}$ as the energy increases. At low energy, the momentum transfer cross section is dominated by elastic scattering. However, as can be seen from Fig. 8, the contribution of inelastic scattering increases at high energy and the inelastic momentum cross section becomes larger than the elastic at energies above 10^3 cm^{-1}. At these energies, the cross sections for different initial rotational levels become very similar.

C. Rate coefficients

The scattering rate coefficients (11) are presented in Fig. 9(a) for temperatures between 1 and 1000 K and for the initial rotational levels $j = 1$, $j = 5$, and $j = 10$. The elastic rates k_{jj} are very similar for the three initial rotational levels and grow with increasing temperature. The inelastic rates (summed over all final rotational levels $j' \neq j$) are displayed in the same figure. The rates are consistent with the cross sections discussed above (see Fig. 7) and increase with T. Over the whole range of temperatures considered, the rate coefficients are dominated by elastic collisions, as expected from the previous discussion. The momentum transfer rates for initial rotational levels $j = 1$, 5, and 10 are shown in Fig. 9(b). The elastic rates have comparable magnitudes, although they differ by as much as 50% at $T = 1$ K. The elastic momentum transfer rate for $j = 1$ increases from 1 K to 16 K, where it reaches a maximum, and then decreases from 16 K to 1000 K. The rate for the initial rotational levels $j = 5$ and $j = 10$ presents a similar behavior, but the maximum is shifted toward higher temperatures. The elastic momentum transfer rates are smaller than the scattering rates, and the difference between the two types of rates increases from a factor of 3 at $T = 1$ K to a factor of 25 at $T = 1000$ K. This reflects the fact that the elastic momentum transfer cross sections decrease more rapidly than the scattering cross sections when the energy increases. On the other hand, the inelastic momentum transfer rates are very similar to the inelastic scattering rates, so that inelastic transitions play a much more important role for momentum transfer rates at high temperatures. This behavior was also observed in the case of Na–N_2 collisions.[3] At temperatures of 1000 K and above, the inelastic momentum transfer rates are in fact larger than the elastic rates.

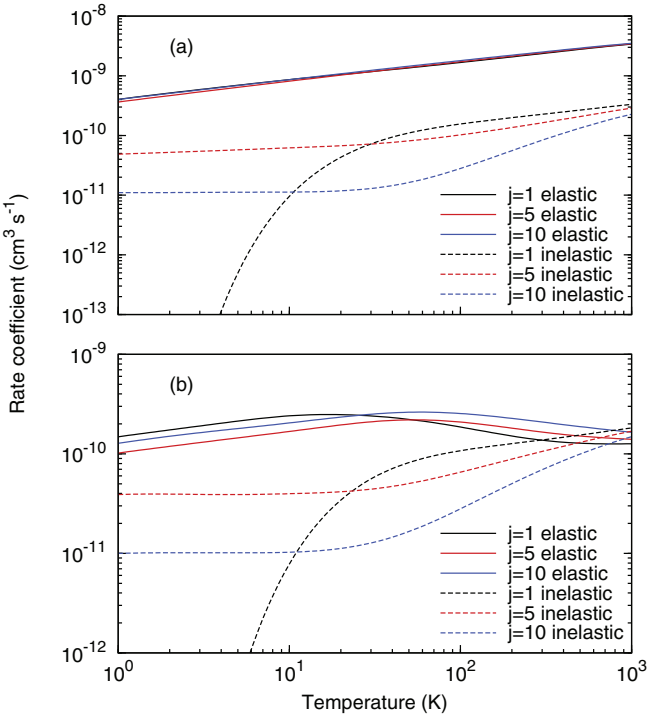

FIG. 9. Rates coefficients for Ag–N_2 collisions as a function of the temperature for the three initial rotational levels $j = 1$, $j = 5$, and $j = 10$. (a) Scattering rate coefficients; (b) momentum transfer rate coefficients. Full lines: elastic collisions; dashed lines: inelastic collisions.

D. Comparison with Na–N_2 scattering

As Ag has been suggested as a proxy for Na in experiments with N_2 and O_2,[4] it is useful to compare the collisional properties of both species with N_2. In Fig. 10, we show a comparison of the scattering cross sections and the rate coefficients for the initial rotational level $j = 5$. We have extended the results of our previous calculations on Na–N_2 collisions for energies down to 0.1 cm^{-1} and up to 5000 cm^{-1} in order to be able to compare the cross sections (rates) over a large

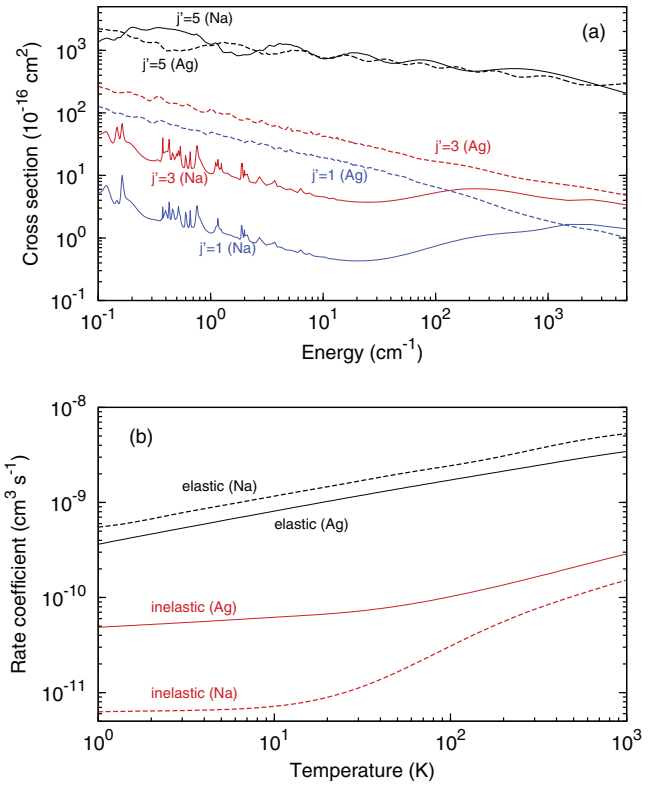

FIG. 10. Comparison between (a) the scattering cross sections, and (b) the scattering rate coefficients, in collision of Ag or Na with $N_2(j = 5)$. The value of the final rotational level j' is indicated next to each curve and the colliding atom in indicated in parentheses. Panel (a) shows the elastic cross section as well as the relaxation cross sections. Panel (b) shows the elastic and inelastic (including excitation) rate coefficients.

range of energies (temperatures). As illustrated in Fig. 10(a), the elastic cross sections for both processes are of the same magnitude, while the inelastic cross sections are much more important in the case of Ag–N_2 collisions at low energy. At energies larger than 10^3 cm^{-1}, the relaxation cross sections become similar for the two systems. This can be explained by observing that the van der Waals potential for AgN_2 is more anisotropic than in the case of NaN_2, which can be seen clearly by comparing the radial functions V_λ for both complexes (see Fig. 2 and Fig. 2 of Ref. 3). We observe that at low energy, the terms with $\lambda \neq 0$ are larger for the AgN_2 complex than for NaN_2 in the classically allowed region, therefore, favoring inelastic transitions in the former system. This discussion is also valid for the momentum transfer cross sections.

The scattering rate coefficients, shown in Fig. 10(b), reflect the above discussion on the cross sections. At the lowest temperature considered in this work ($T = 1$ K), the inelastic rate for Ag–N_2 collisions is larger than the rate for Na–N_2 by an order of magnitude, while at $T = 1000$ K the difference is about a factor of 2. On the other hand, the elastic rate for Na–N_2 is larger than for Ag–N_2. This is mainly due to the fact that the reduced mass of the system, which is larger for AgN_2, appears in the calculation of the rate coefficient (see Eq. (11)). The total rate (obtained by summing the elastic and inelastic rates) for the two collisional complexes is also very similar. If the mass difference between the two systems is neglected, we find that the rates for Na–N_2 and Ag–N_2 collisions differ by at most 10% over the range of temperatures considered in this work. Therefore, while the contributions of elastic and inelastic transitions are quite different, we conclude that the total rate coefficient for Ag–N_2 collisions can be obtained simply by scaling the rate for Na–N_2 collisions by the square root of the ratio of the reduced masses of the two systems. These findings are also valid in the case of the momentum transfer rate coefficients, except that the difference between the total rates is of at most 15% instead of 10%.

IV. CONCLUSIONS

We have performed a quantal study of elastic and inelastic rotational collisions of Ag with N_2 for collision energies between 0.1 and 5000 cm^{-1}. We have obtained the two-dimensional PES of the ground state of the AgN_2 complex by means of the coupled-cluster method implemented in MOLPRO with the N_2 internuclear distance fixed to its equilibrium geometry. The potential has a minimum at the geometry $R = 8.13$ a.u. and $\theta = 127.2°$, while the maximum depth of the well is 81.8 cm^{-1}. The asymptotic part of the potential was constructed analytically by calculating the C_6 dispersion coefficient.

We investigated the Ag–N_2 collisions using the quantum-mechanical close-coupling method for energies between 0.1 and 5000 cm^{-1}. We calculated the cross sections for elastic scattering, as well as for rotational excitation and relaxation, for various initial rotational levels. Over the range of energies considered in this work, the elastic cross sections are about an order of magnitude larger than the inelastic cross sections. The elastic cross sections present a complicated resonance structure, which depends on the initial rotational level j for energies below the depth of the potential well, while for energies above 80 cm^{-1} the elastic cross sections are very similar for all values of j. The inelastic cross sections, on the other hand, decrease with increasing initial rotational level but become independent of j at high energy. The elastic momentum transfer cross sections are smaller than the scattering cross section, and the difference between the two types of cross sections increases with energy. However, this is not the case for the inelastic momentum transfer cross sections, so that at high energy the momentum transfer occurs primarily through inelastic collisions. Finally, we calculated the elastic and inelastic rate coefficients for temperatures between 1 K and 1000 K. The elastic scattering rate increases with the temperature, while the elastic momentum transfer rate increases until it reaches a maximum at a temperature, which depends on the initial rotational level, and then decreases at higher temperatures.

ACKNOWLEDGMENTS

The authors would like to thank D. Budker for useful discussions as well as J. Mitroy and H. Sadeghpour for providing us with the dynamical electric dipole polarizabilities for the Ag atom. J.L. is supported by a fellowship from the Belgian American Educational Foundation, and the research of A.D. and P.Z. is supported by the Chemical Science, Geoscience, and Bioscience Division of the Office of Basic Energy Science, Office of Science, U.S. Department of Energy.

[1] R. Holzlöhner, S. Rochester, D. Bonaccini Calia, D. Budker, J. Higbie, and W. Hackenberg, Astron. Astrophys. **510**, A20 (2010).
[2] J. Higbie, S. Rochester, B. Patton, R. Holzlöhner, D. Bonaccini Calia, and D. Budker, Proc. Natl. Acad. Sci. U.S.A. **108**, 3522 (2011).
[3] J. Loreau, P. Zhang, and A. Dalgarno, J. Chem. Phys. **135**, 174301 (2011).
[4] D. Budker, private communication (2011).
[5] A. Sushkov and D. Budker, Phys. Rev. A **77**, 042707 (2008).
[6] T. Tscherbul, P. Zhang, H. R. Sadeghpour, and A. Dalgarno, Phys. Rev. Lett. **107**, 023204 (2011).
[7] T. Walker and W. Happer, Rev. Mod. Phys. **69**, 629 (1997).
[8] B. Lancor, E. Babcock, R. Wyllie, and T. Walker, Phys. Rev. Lett. **105**, 083003 (2010).
[9] J. Bendtsen, J. Raman Spectrosc. **2**, 133 (1974).
[10] P. J. Knowles, C. Hampel and H.-J. Werner, J. Chem. Phys. **99**, 5219 (1993).
[11] J. D. Watts, J. Gauss, and R. J. Bartlett, J. Chem. Phys. **98**, 8718 (1993).
[12] H.-J. Werner, P. J. Knowles, R. Lindh, F. R. Manby, M. Schütz *et al.*, MOLPRO, version 2009.1, a package of *ab initio* programs, 2009, see http://www.molpro.net.
[13] K. Peterson and C. Puzzarini, Theor. Chem. Acc. **114**, 283 (2005).
[14] D. Figgen, G. Rauhut, M. Dolg, and H. Stoll, Chem. Phys. **311**, 227 (2005).
[15] T. H. Dunning Jr., J. Chem. Phys. **90**, 1007 (1989).
[16] S. Boys and F. Bernardi, Mol. Phys. **19**, 553 (1970).
[17] A. J. Stone, *The Theory of Intermolecular Forces* (Clarendon, 1997).
[18] D. M. Bishop and J. Pipin, J. Chem. Phys. **97**, 3375 (1992).
[19] R. Moszynski, P. S. Zuchowski, and B. Jezioski, Collect. Czech. Chem. Commun. **70**, 1109 (2005); T. Korona, M. Przybytek, and B. Jeziorski, Mol. Phys. **104**, 2303 (2006).
[20] A. K. Wilson, T. V. Mourik, and T. H. Dunning Jr., J. Mol. Struct.: THEOCHEM **388**, 339 (1996).
[21] J. Zhang, J. Mitroy, H. R. Sadeghpour, and M. Bromley, Phys. Rev. A **78**, 062710 (2008).
[22] A. Arthurs and A. Dalgarno, Proc. R. Soc. London, Ser. A **256**, 540 (1960).
[23] D. R. Flower, *Molecular Collisions in the Interstellar Medium*, 2nd ed. (Cambridge University Press, Cambridge, 2007).
[24] A. Lothus and P. Krupenie, J. Phys. Chem. Ref. Data **6**, 113 (1977).

[25]G. Parker and R. Pack, J. Chem. Phys. **68**, 1585 (1978).
[26]J. M. Hutson and S. Green, MOLSCAT computer code, version 14, distributed by Collaborative Computational Project No. 6 of the Engineering and Physical Sciences Research Council (UK), 1994.
[27]D. Manolopoulos and M. Alexander, J. Chem. Phys. **86**, 2044 (1987).
[28]P. G. Burke, D. Scrutton, J. H. Tait, and A. J. Taylor, J. Phys. B **2**, 1155 (1969).
[29]J. T. Muckerman and R. B. Bernstein, Chem. Phys. Lett. **4**, 183 (1969).
[30]L. N. Smith, D. J. Malik, and D. Secrest, J. Chem. Phys. **71**, 4502 (1979).
[31]R. B. Bernstein, Adv. Chem. Phys. **10**, 75 (1966).
[32]L. D. Landau and E. M. Lifshitz, *Quantum Mechanics: Non-relativistic Theory* (Pergamon, 1997).